

High-precision low-velocity gas measurement via synchronous baseline fitting and flow inhomogeneity analysis in TDLAS

Xin Wang(王鑫), Naihe Song(宋乃禾), Guodong Wang(王国栋), Yanjun Ding(丁艳军), Zhimin Peng(彭志敏), Fang Fang(房方), Yanjun Du(杜艳君)

Citation: Chin. Phys. B. 35, 094205 (2026). DOI: 10.1088/1674-1056/ae1eff | CSTR: 32038.14.CPB.ae1eff
http://cpb.iphy.ac.cn; http://iopscience.iop.org/cpb

What follows is a list of articles you may be interested in

Dual-attention cGAN for high-fidelity ghost imaging at ultra-low sampling rates

Yuanyuan Ma(马园园), Yunfan He(何运繁), Le Wang(王乐), Shengmei Zhao(赵生妹)
Chin. Phys. B. 35, 094207 (2026). DOI: 10.1088/1674-1056/ae1b78 | CSTR: 32038.14.CPB.ae1b78

Tunable terahertz slow-light device based on triple plasmon-induced transparency on a patterned graphene metasurface

Bo-Yun Wang(王波云), Yao-Yang Dai(代耀阳), De-Bing Long(龙德兵), Hua-Qing Yu(余华清)
Chin. Phys. B. 35, 084211 (2026). DOI: 10.1088/1674-1056/ae86db | CSTR: 32038.14.CPB.ae86db

A full-chain simulation model for electron-bombarded active pixel sensors in low-light imaging

Zhen-Yuan Zhu(朱振源), Jing-Zhi Zhang(张景智), Yun-Sheng Qian(钱芸生), Yi-Jun Zhang(张益军), Yi-Lun Wang(王逸伦), Gang-Cheng Jiao(焦岗成)
Chin. Phys. B. 35, 084208 (2026). DOI: 10.1088/1674-1056/ae1725 | CSTR: 32038.14.CPB.ae1725

Self-calibration wavelength modulation spectroscopy for acetylene detection based on tunable diode laser absorption spectroscopy

Qin-Bin Huang(黄秦斌), Xue-Mei Xu(许雪梅), Chen-Jing Li(李晨静), Yi-Peng Ding(丁一鹏), Can Cao(曹粲), Lin-Zi Yin(尹林子), Jia-Feng Ding(丁家峰)
Chin. Phys. B. 25, 114202 (2016). DOI: 10.1088/1674-1056/25/11/114202

Analysis of algebraic reconstruction technique for accurate imaging of gas temperature and concentration based on tunable diode laser absorption spectroscopy

Hui-Hui Xia(夏晖晖), Rui-Feng Kan(阚瑞峰), Jian-Guo Liu(刘建国), Zhen-Yu Xu(许振宇), Ya-Bai He(何亚柏)
Chin. Phys. B. 25, 064205 (2016). DOI: 10.1088/1674-1056/25/6/064205

High-precision low-velocity gas measurement via synchronous baseline fitting and flow inhomogeneity analysis in TDLAS

Xin Wang(王鑫)[1], Naihe Song(宋乃禾)[2], Guodong Wang(王国栋)[1], Yanjun Ding(丁艳军)[2], Zhimin Peng(彭志敏)[2], Fang Fang(房方)[1], and Yanjun Du(杜艳君)[1,†]

[1] *School of Control and Computer Engineering, North China Electric Power University, Beijing* 102206, *China*
[2] *Department of Energy and Power Engineering, Tsinghua University, Beijing* 100084, *China*

(Received 4 September 2025; revised manuscript received 27 October 2025; accepted manuscript online 13 November 2025)

Accurate measurement of gas flow velocities in low-speed flow fields (0–30 m/s) is critical for applications such as vacuum drying, semiconductor manufacturing, and pharmaceutical/food industries. Based on the laser Doppler effect, non-contact high-precision measurement of gas flow velocity can be achieved by capturing the Doppler shift in absorption spectral lines to quantify the gas flow speed. However, under low-speed flow field conditions, weak Doppler shifts (on the order of 10^{-5} cm^{-1} per m/s) and spectral line overlapping pose significant challenges to traditional direct absorption spectroscopy (DAS). To address these issues, this study employs a dual-light-path system based on tunable diode laser absorption spectroscopy (TDLAS) and proposes a synchronous iterative fitting algorithm with an L2-norm constraint. This algorithm simultaneously optimizes the baseline and absorption line parameters, effectively eliminating baseline drift and spectral line interference inherent in traditional DAS. Additionally, we analyze the non-uniformity of turbulent flow fields in pipes and model the radial velocity profile using a power-law distribution to elucidate its impact on TDLAS path-averaged velocity measurements. We ensure the reliability of the results by analyzing the effects of turbulence, spectral line distortion caused by stagnant zones, and zero-point deviation during measurements. Using the H_2O absorption line at 7181.1557 cm^{-1}, the proposed method measures velocities in the range of 0–25.42 m/s with a relative error of less than 1%. The measurement results exhibit high linearity against reference results under the same conditions, indicating excellent system consistency. This research provides theoretical guidance and technical support for the engineering application of TDLAS in low-speed flow field measurements.

Keywords: tunable diode laser absorption spectroscopy (TDLAS), low-velocity measurement, synchronous iterative fitting, doppler shift, flow field non-uniformity

PACS: 42.87.–d, 52.70.Kz, 07.07.Df

DOI: 10.1088/1674-1056/ae1eff **CSTR:** 32038.14.CPB.ae1eff

1. Introduction

Low-speed flow fields are gaining increasing attention in energy, environmental, and semiconductor manufacturing and biopharmaceutical processes. Compared to high-speed flows dominated by turbulent characteristics and inertial forces, low-speed flows exhibit greater susceptibility to viscous forces and external environmental factors, resulting in complex flow regimes with heightened sensitivity to measurement disturbances.[1,2] Traditional intrusive probes often fail to deliver stable measurements in small-scale, high-humidity, or corrosive environments due to inadequate reliability and measurement accuracy.[3,4] Meanwhile, alternative non-contact techniques, such as particle-dependent velocimetry methods like laser Doppler velocimetry (LDV) and particle image velocimetry (PIV), suffer from severely degraded signal-to-noise ratios in low-speed flows owing to insufficient tracer particle concentrations or particle sedimentation.[5,6]

Tunable diode laser absorption spectroscopy (TDLAS) offers distinct advantages including rapid measurement speed, high sensitivity, strong selectivity, and non-invasiveness. This technique employs a tunable semiconductor laser (distributed feedback, DFB laser) to scan specific wavelengths, detecting selective absorption characteristics of gas molecules.[7] The velocity of gas flow can be measured by detecting the Doppler shift of the central wavelength of the absorption spectral line. Integrating Doppler shift measurements with multi-path absorption methods and high-precision spectral fitting algorithms further enhances spatial resolution in velocity measurements. Leveraging these strengths, TDLAS has been extensively applied in flow field diagnostics.[8,9] Philippe *et al.* (1993) pioneered its implementation in shock tube flow measurements, validating feasibility for high-speed flows.[10] Subsequent studies by Wehe *et al.* (1998) and Yang Bin *et al.* (2011) expanded its application scope to supersonic wind tunnels and air-breathing engine diagnostics, respectively.[11,12] Recently, Tu *et al.* (2022) achieved high-precision measurements (relative error $< 4.3\%$) within the range of 700 m/s–1000 m/s using a dual-light-path system.[13] Lu *et al.* (2024) developed a WMS-based velocity measurement method using even-symmetric $2f/1f$ harmonics, demonstrating improved

†Corresponding author. E-mail: yanjundu@ncepu.edu.cn

© 2026 Chinese Physical Society and IOP Publishing Ltd. All rights, including for text and data mining, AI training, and similar technologies, are reserved.

precision with a velocity standard deviation of 15.6 m/s in turbojet engine exhaust measurements.[14] Zhou *et al*. (2025) proposed a non-absorption-loss immune TDLAS sensor achieving an SNR improvement of 6.46 dB in Mach 2.8 supersonic flows with measurement errors below 1.39%.[15]

Research on low-speed flow measurements remains relatively limited, with many prior efforts relying on wavelength modulation spectroscopy (WMS) to improve signal-to-noise ratio. For instance, studies conducted under well-controlled conditions, such as in idealized low-speed wind tunnels (0 m/s–23 m/s) equipped with flow uniformity screens, have reported velocity uncertainties below 1 m/s. Nevertheless, the practical application of WMS entails certain challenges, including sensitivity to modulation parameters (*e.g*. depth and frequency) that can introduce harmonic distortion. High-frequency modulation may also exacerbate laser nonlinearities, which contributes to uncertainty in estimating harmonic center frequency shifts.[16,17] Additionally, achieving strict synchronization across multiple signal channels remains difficult, often resulting in phase discrepancies that further affect the accuracy of frequency-based measurements. In contrast, direct absorption spectroscopy (DAS) offers structural simplicity and operational convenience through direct acquisition of complete absorption lineshapes. Nevertheless, the minuscule Doppler shifts in low-speed flows ($\sim 3.59 \times 10^{-5}$ cm^{-1} per m/s) impose extreme demands on spectral fitting precision. Traditional DAS techniques, constrained by insufficient signal-to-noise ratios and baseline extraction inaccuracies, fail to meet the rigorous requirements for reliable low-speed flow diagnostics.

To address this precision bottleneck arising from weak Doppler shifts and spectral line overlapping in low-speed flow measurements, this study proposes a synchronous iterative fitting algorithm with rigorous baseline extraction. A dual-light-path system targeting the H_2O absorption line at 7181.1557 cm^{-1} (near-infrared region) is used to validate the proposed method. By simultaneously optimizing baseline and absorption line parameters, our method effectively eliminates baseline drift and resolves spectral interference, thereby reducing flow velocity measurement relative errors to below 12%. Leveraging the Doppler effect through a cross-light-path configuration, we extract differential frequency shifts of identical spectral lines, enabling high-precision velocity measurements in a range of 0 m/s–25.84 m/s. Moreover, not only the velocity, but also other gas parameters, such as concentration, can be derived together in the spectral fitting. This highlights that the proposed method has the ability for real-time multi-parameter monitoring. This work systematically analyzes critical technical details and measurement uncertainties, providing a robust solution for TDLAS engineering applications in low-speed flow diagnostics.

2. TDLAS flow velocity measurement principle

2.1. Laser doppler effect

The fundamental principle underlying TDLAS flow velocity measurement is based on the laser Doppler effect. Within a flow field, gas molecules undergo two primary types of motion: random thermal motion (responsible for Doppler broadening of spectral lines) and directed bulk motion (responsible for a frequency shift in the absorption spectrum). This combined effect encodes information about the gas velocity distribution.[18]

The Doppler effect manifests when relative motion exists between the observer (here, the gas molecules) and the laser. Therefore, the flow velocity can be determined by measuring the laser's Doppler shift.[19] For incident light at frequency v, the frequency v perceived by moving gas molecules is

$$\nu = \nu_0 \pm \Delta\nu = \nu_0 \left(1 \pm \frac{V}{c}\right), \tag{1}$$

where V is the velocity component of the gas molecules along the laser propagation direction, c denotes the speed of light, and $\Delta\nu$ represents the Doppler frequency shift, with its sign indicating the molecular motion along the laser propagation direction ($+$ for approaching, $-$ for receding). Within the TDLAS measurement framework, the conventional approach involves directing a laser beam through the flow field at a specific angle and comparing its spectral characteristics with those of a reference laser at zero flow velocity.[20] However, in low-velocity flow fields, the Doppler shift induced by the gas flow is extremely weak, making the frequency shift signal challenging to detect. To address this, the present study employs a symmetric crossed-beam configuration: two laser beams traverse the flow field at symmetric angles θ relative to the normal of the main flow direction, as shown in Fig. 1. In this configuration, the relative motion between the absorbing molecules and the laser beam propagation direction causes an effective advancement or delay in the photon absorption process, resulting in opposite-direction frequency shifts in the absorption spectra of the two laser beams (*i.e*., one exhibiting a redshift and the other a blueshift). This approach doubles the detectable Doppler shift magnitude, significantly enhancing the precision of velocity measurements. The center frequency shift $\Delta\nu$ of the fitted absorption spectral line is proportional to the projected velocity V_{Dop} along the beam direction, and its quantitative relationship with the true gas flow velocity V_{gas} is given by

$$V_{\mathrm{gas}} = \frac{V_{\mathrm{Dop}}}{\sin\theta} = \frac{c \cdot \Delta\nu}{2 \cdot \nu_0 \cdot \sin\theta}. \tag{2}$$

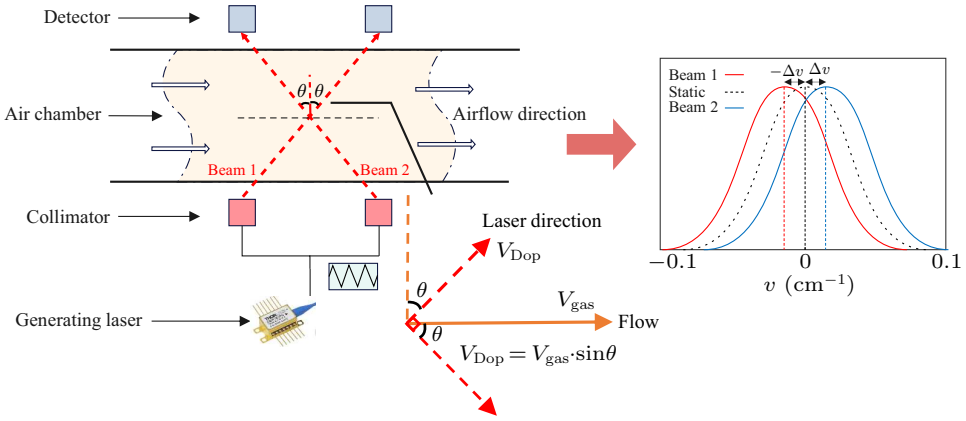


Fig. 1. Schematic diagram of Doppler shift in absorption spectra.

Notably, the spectral frequency shift depends only on the molecular velocity vector, not on absorption conditions (*e.g.*, water vapor mole fraction, temperature). Since our method measures the relative shift between two beams in the same flow field, consistent absorption conditions across experiments are not required.

Water molecules, abundant in atmospheric environments and a primary combustion product of hydrocarbons, exhibit strong absorption characteristics in the near-infrared spectrum. Consequently, they serve as widely adopted tracer molecules for flow velocity measurements. However, the complex absorption line structure of H_2O introduces inevitable interference between the target and its adjacent spectral lines. Through systematic spectral screening, this study selects the 7181.1557 cm^{-1} line as the target transition. Figure 2 illustrates the absorption characteristics of H_2O under standard conditions, revealing partial overlap between neighboring interference lines and the primary absorption peak. Such overlap degrades absorption line fitting accuracy and consequently compromises Doppler shift detection precision. To mitigate these effects, the next section introduces a synchronous iterative fitting algorithm.

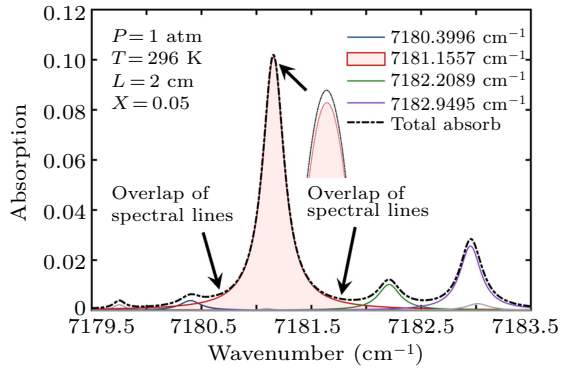


Fig. 2. Multi-line absorption of H_2O near 7181.1557 cm^{-1}. The unit 1 atm = 1.01325×10^5 Pa.

2.2. Synchronous iterative fitting approach

When an infrared laser of frequency v traverses an absorbing flow field medium of path length L, the transmitted intensity $I(t)$ relates to the incident intensity $I(t)$ according to the Beer–Lambert law:

$$I_t(t) = I_0(t)\exp\left(-\int_0^L P\cdot X(x)\cdot S[T(x)]\cdot\phi[\nu(t)]\,\mathrm{d}x\right), \quad (3)$$

where P, X, and T represent the local pressure, mole fraction, and temperature of the target gas medium, respectively; $S(T)$ denotes the temperature-dependent absorption line strength; and $\phi(v)$ is the lineshape function.

DAS, as a primary implementation method for TDLAS, directly acquires complete absorption spectra through laser wavelength scanning. For most species concentration measurements, which target extracting the integrated area of the absorption, the non-absorbing baseline I_0 is conventionally approximated by polynomial fitting of non-absorbing spectral regions.[19] However, for flow velocity measurements, where the overall absorption line profiles (line-shape and line-center) need to be obtained with high accuracy, the conventional baseline estimation method is not applicable. As shown in Fig. 2, the target absorption line at 7181.1557 cm^{-1} inevitably overlaps with neighboring interference lines. Traditional methods assume zero absorption at the scan edges and use these regions for baseline fitting. However, when residual absorption from neighboring lines exists at the edges, the transmitted light intensity has already been attenuated. Traditional methods mistakenly use these attenuated points as baseline references, leading to systematic underestimation of I_0 (as illustrated in Fig. 9(b) where the traditional baseline lies below the synchronous baseline in shaded overlap regions). This baseline error propagates into the absorption lineshape fitting and causes biased center frequency extraction, which is particularly problematic for low-velocity measurements where weak Doppler shifts must be accurately resolved. Therefore, we propose a synchronous fitting approach that concurrently optimizes the baseline and absorption feature.

Based on a careful examination of the laser output, the baseline can be modeled by a j-th-order polynomial in time

domain:

$$I_0(t) = \sum_{n=0}^{j} a_n t^n, \tag{4}$$

where a_n denotes the polynomial coefficients, with the polynomial degree j determined by the characteristics of the distributed feedback laser. This study employs a quadratic polynomial for fitting.

With the assumption of a uniform absorbing gas medium along the light path, the absorption coefficient can be expressed

$$\alpha(\nu(t)) = P \cdot L \cdot S(T) \cdot L \cdot \phi(\nu) = A \cdot \phi(\nu), \tag{5}$$

where A is the integrated absorbance. As for the lineshape, the Voigt profile, defined as the convolution of Gaussian (Doppler broadening $\Delta\nu_{\mathrm{D}}$) and Lorentzian (collisional broadening $\Delta\nu_{\mathrm{C}}$) profiles, is adopted

$$\phi(\nu) = \frac{2}{\Delta\nu_D}\sqrt{\frac{\ln 2}{\pi}}\frac{a}{\pi}\int_{-\infty}^{\infty}\frac{\exp\left(-y^2\right)}{a^2+(\omega-y)^2}\,\mathrm{d}y, \tag{6}$$

where $a = \sqrt{\ln 2}\Delta\nu_{\mathrm{C}}/\Delta\nu_{\mathrm{D}}$ and $w = 2\sqrt{\ln 2}(\nu - \nu_0 - \Delta\nu)/\Delta\nu_{\mathrm{D}}$, ν_0 is the central wavenumber, $\Delta\nu$ represents the Doppler shift. With a linear (sawtooth) scan of the injected laser current, the laser wavelength can be described as follows:

$$\nu(t) = \sum_{i=0}^{2} m_i t^i, \tag{7}$$

where coefficients m_i describe the time-dependent variation of the laser wavenumber. These coefficients are determined through etalon calibration: a Fabry–Pérot interferometer with known free spectral range generates periodic interference peaks in the time domain, which serve as frequency markers to establish the time-to-wavenumber conversion relationship. This calibration procedure is illustrated in Fig. 9(a), where the interference peaks are used to transform the transmitted intensity from the time domain to the frequency domain.[22]

The optimization process employs an L2-norm-constraint objective function to minimize the residuals between the detected transmitted light intensity and the simulated one[23]

$$F(t) = \left\| I_t(t) - I_0(t, a_i) \times \exp\left[-\alpha(\nu(t), \Delta\nu, \Delta\nu_C, A)\right] \right\|_2, \tag{8}$$

where $I_t(t)$ and $I_0(t, a_i)$ represent the measured light intensity and the fitted baseline, respectively, with $\{a_i, \Delta\nu, \Delta\nu_{\mathrm{C}}, A\}$ as the parameters to be fitted. Under constant temperature conditions, the collisional broadening $\Delta\nu_{\mathrm{D}}$ can be calculated using a database. At the minimum of $F(t)$, optimal values for flow field parameters and baseline coefficients are obtained, effectively eliminating baseline drift and resolving spectral interference.

2.3. Algorithm

The flow field parameter extraction process using transmitted light intensity and synchronous fitting comprises the following two main steps (Fig. 3).

Step 1: Initial parameter estimation

The initial phase involves extracting the quasi-non-absorbing baseline from the transmitted intensity signal to perform preliminary baseline fitting. This provides initial baseline parameters while enabling calculation of approximate absorbance and Doppler broadening values. Concurrently, wavelength scanning calibration establishes the time-wavenumber conversion relationship and determines the wavenumber zero-point offset, with convergence tolerance e defined.

Step 2: Iterative optimization

Based on the current set of parameters, the baseline and absorption line shapes are computed in the time domain. The simulated transmitted intensity is then computed and compared against measured data through the L2-norm error function. If the error satisfies tolerance e, the iteration process stops and the current flow parameters become the result; otherwise, parameters are updated and the process iterates. Finally, the relative Doppler shift is determined from differential frequency shifts of the dual spectral lines, enabling flow velocity calculation via Eq. (2).

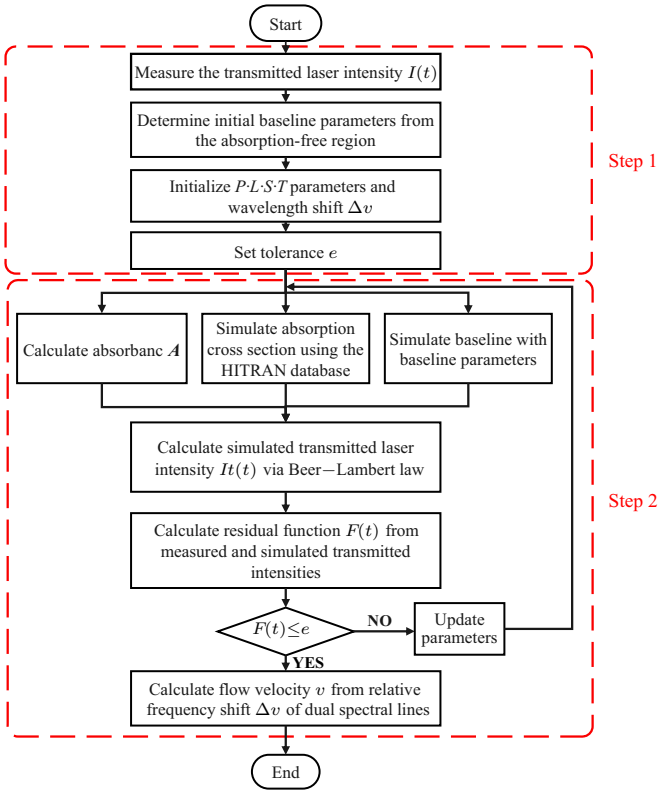


Fig. 3. Flowchart for extracting flow field gas parameters.

3. Measurement system

The experimental system in Fig. 4 was constructed to validate the feasibility of TDLAS for gas velocity measurement

in low-speed flow fields. The system comprises three modules: (i) the laser sensing module, (ii) the flow field generation module, and (iii) the signal processing module. In the laser sensing module, a signal generator (KEYSIGHT TECHNOLOGIES, 335500B) outputs a 1000-Hz sawtooth modulation signal (200 mVpp) to drive a distributed feedback laser controller (THORLABS, ITC4001) via current tuning. This generates a laser wavelength scan in the range 7180.58 cm^{-1}–7181.66 cm^{-1} where the H_2O transition was measured. The output laser was divided by a beam splitter into three beams (power ratio 3:3:4): one beam illuminates a Fabry–Pérot (THORLABS, SA200-2B) interferometer etalon (free spectral range: 0.05 cm^{-1}) for relative wavelength calibration, while the other two beams intersect within the flow field test area to acquire target absorption spectra. The signal processing module comprises a data acquisition card (PCIE8536C,ART) integrated with a LabVIEW-based real-time processing system. Detector signals are transmitted to the computer via the data acquisition card, where the synchronous iterative fitting algorithm described in Subsection 2.3 continuously analyzes the light intensity signals to extract flow velocity information in real time. The entire procedure, from signal acquisition to the completion of data processing, is completed within approximately 0.25 s, enabling continuous data acquisition for extended validation studies.

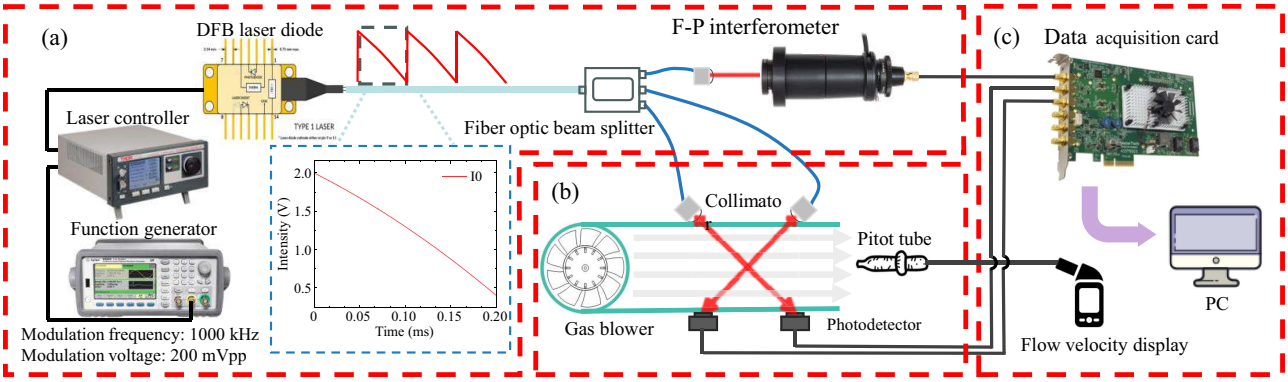


Fig. 4. TDLAS low-speed flow field measurement system: (a) laser detection module, (b) flow field generation module, (c) signal processing module.

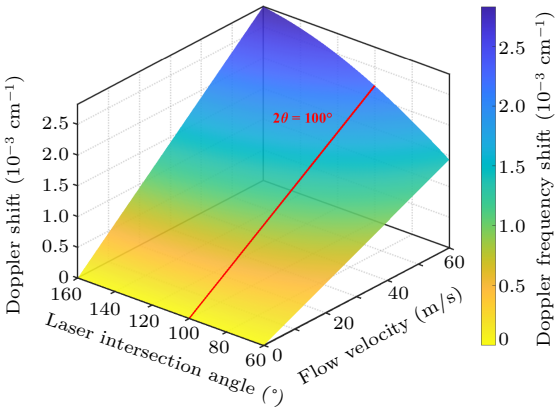


Fig. 5. Theoretical Doppler shift *versus* laser angle in TDLAS.

The flow field generation module employs a low-power fan coupled with a cylindrical glass wind tunnel (diameter: 2 cm, length: 40 cm) to establish adjustable low-speed flows. Transparent tube walls facilitate optical transmission, and the working medium is clean air under standard conditions (25 °C, 101.325 kPa). A zero-velocity flow field serves as a reference for phase noise evaluation and system background calibration. Based on Eq. (2), the Doppler shift with different flow velocity at varying laser angles can be calculated, as shown in Fig. 5. Although the shift increases with the crossing angle, due to layout constraints and reflective interference from glass windows, the optimal beam-crossing angle was determined as $2\theta = 100°$. At this angle, a 1-m/s velocity increment corresponds to a Doppler shift of 3.693×10^{-5} cm^{-1}, while a 100-m/s flow induces shifts of 10^{-4} cm^{-1}–10^{-3} cm^{-1}. An S-type Pitot tube probe is fixed at the wind tunnel outlet center to measure maximum centerline velocity V_{max}, serving the result verification purpose.

4. Discussion

4.1. Analysis of pipe flow field non-uniformity

Since TDLAS yields a path-averaged velocity while the Pitot tube provides a point measurement, aerodynamic analysis of the pipe flow field was conducted to ensure accurate comparison and to evaluate the impact of the velocity profile on TDLAS path-averaged velocity measurements. For flow velocities ranging from 5 m/s to 30 m/s, the Reynolds number ($Re = \rho V D/\mu$) spans 6.6×10^3 to 3.96×10^4, exceeding the critical threshold for laminar-to-turbulent transition ($Re_{crit} \approx 4000$), confirming turbulent flow conditions.[24] To address the entrance effect, the hydrodynamic entrance length (L_e) for fully developed turbulent flow was calculated using the empirical correlation $L_e/D \approx 4.4Re^{1/6}$.[25] For $Re = 6.6 \times 10^3$, $L_e/D \approx 16.7$, and for $Re = 3.96 \times 10^4$, $L_e/D \approx 22.9$. Given the wind tunnel configuration with $L/D = 20$ (length 40 cm, diameter 2 cm), the flow is fully developed at lower Re values ($L > L_e$) but may retain minor developing flow characteristics at higher Re (L slightly $< L_e$). This could lead to a slightly

flatter velocity profile in the entrance region, potentially overestimating the path-averaged velocity by approximately 2%–5% due to thinner boundary layers.[26] However, as the laser beams intersect near the tunnel terminus, the entrance effect is considered negligible for our analysis, justifying the assumption of fully developed turbulent flow. The radial velocity distribution was modeled using the power-law profile to determine the true radial average velocity. The high linearity of the experimental results (see Fig. 12) further validates the reasonableness of this assumption.

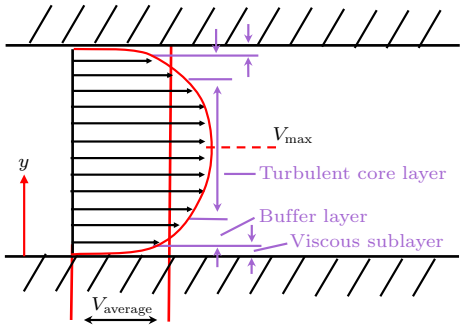


Fig. 6. Velocity structure of turbulent pipe flow.

Fully developed turbulent pipe flow (Fig. 6) features a velocity structure comprising three distinct regions: the turbulent core in the central region, dominated by irregular turbulent fluctuations and momentum transfer primarily governed by turbulent shear stress; the viscous sublayer adjacent to the pipe wall, where viscous forces prevail, exhibiting smooth laminar-like flow with momentum losses determined mainly by viscous shear stress; and the transition layer connecting these two regions, which exhibits characteristics of both flow regimes. Collectively, the viscous sublayer and transition layer constitute the boundary layer.[27,28]

The radial velocity distribution $V(r)$ in smooth circular pipes under turbulent flow cannot be derived theoretically but is empirically determined by the power-law relationship

$$\frac{V(r)}{V_{\max}} = \left(1 - \frac{r}{R}\right)^n, \tag{9}$$

where r denotes the radial distance from the pipe centerline, R is the pipe radius, $V_{\max}$ represents the maximum velocity at the centerline ($r = 0$), and the exponent n is empirically determined and exhibits a dependence on the Reynolds number Re, as summarized in Table 1.[29]

Table 1. Variation of power-law exponent with Re.

4.0×10^3	2.3×10^4	1.1×10^5	1.1×10^6
1/6.0	1/6.6	1/7.0	1/8.8

The laser beams intercept the pipe at an angle, and the optical paths have a component on the y-axis, resulting in significant non-uniformity of flow velocity along the optical path. This effect is clearly illustrated in the top-view schematic of the TDLAS measurement with boundary layer flow (Fig. 7), where the optical path length traversing the active flow region is $L_{\text{opt}} = 2/\cos\theta$ cm. Perpendicular to the outer pipe wall, there exists an air gap of approximately 1 cm from the wall to the center of the emitter/detector assembly, resulting in a total stagnation region length of $1/\cos\theta$ cm along the optical path. This visualization highlights the pronounced influence of boundary layer and stagnation regions on the velocity distribution sampled by the laser beam.

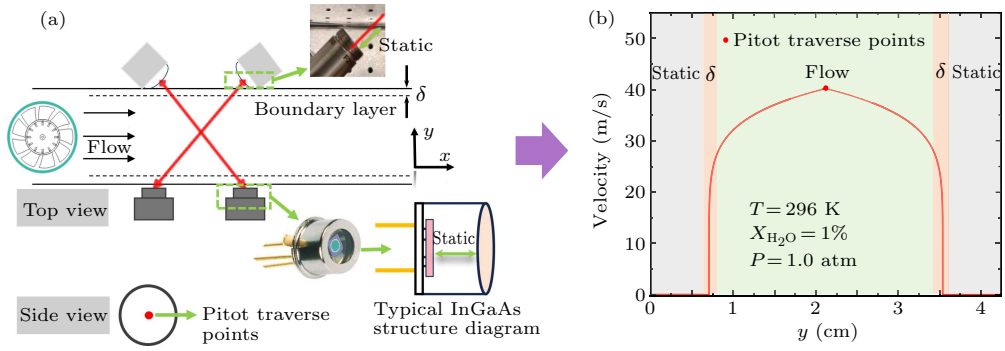


Fig. 7. Effect of boundary layer on TDLAS measurements: (a) top view of velocity distribution, (b) reconstructed radial velocity profile.

The averaged velocity $\bar{V}$ is defined as the integral mean of the velocity distribution along the optical path length. For TDLAS measurement with optical path length L, the path-averaged velocity is expressed as

$$\overline{V} = \frac{1}{L}\int_0^L V(r)\,\mathrm{d}r, \tag{10}$$

where $V(r)$ defines the flow velocity at optical path l position r. The velocity distribution in fully developed turbulent pipe flow is approximated using a power-law model. Substituting the power-law model from Eq. (9) yields

$$\overline{V} = \frac{1}{L}\int_0^L V_{\max}\left(1 - \frac{r}{L}\right)^n \mathrm{d}r. \tag{11}$$

For each experimental flow condition, the corresponding Reynolds number Re was computed, and the specific exponent n was obtained via interpolation using Table 1. Accounting for the stagnant regions near the pipe walls, the complete ra-

dial velocity distribution within the pipe was reconstructed, as shown in Fig. 7(b).[30] Consequently, the reference average velocity used for comparative analysis throughout this study represents this calculated cross-sectional mean velocity $\bar{V}$, conceptually depicted by the integral averaging process in Fig. 8.

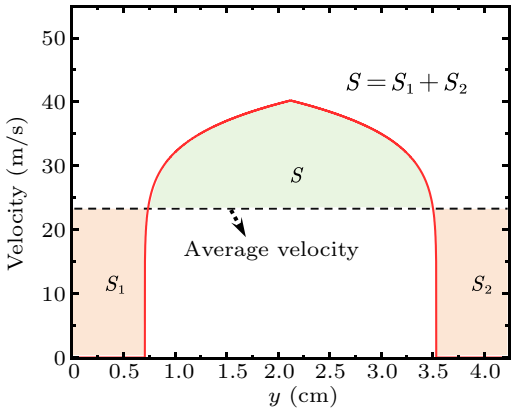


Fig. 8. Integration diagram for reference average velocity.

4.2. Measurement results analysis

Figure 9 shows the raw time-domain signals captured by the oscilloscope (Fig. 9(a)). Through calibration of interference peaks, the light intensity signals of the two laser beams were transformed from the time domain to the frequency domain (Fig. 9(b)), where the frequency interval between adjacent interference peaks is determined by the FSR (free spectral range) of the interferometer. Subsequently, the baseline intensity I_0 was extracted using the synchronous fitting method described in Subsection 2.2. Figure 9(b) demonstrates the baseline misestimation issue in traditional methods under spectral overlap conditions. The shaded regions highlight spectral overlap areas where neighboring lines cause residual absorption. Traditional baselines (dash–dot lines) lie systematically below synchronous baselines (dashed lines) in these regions because they incorrectly use attenuated data points as baseline references, leading to systematic I_0 underestimation. The synchronous method, through simultaneous optimization of baseline and absorption parameters, correctly distinguishes laser output intensity from absorption effects, yielding accurate baseline estimation even in overlap regions. The low fitting residuals (standard deviation 1.8 cm^{-1}–2.3×10^{-4} cm^{-1}) shown in Fig. 10 validate the effectiveness of our synchronous fitting approach in addressing the spectral overlap challenge in low-velocity flow diagnostics.

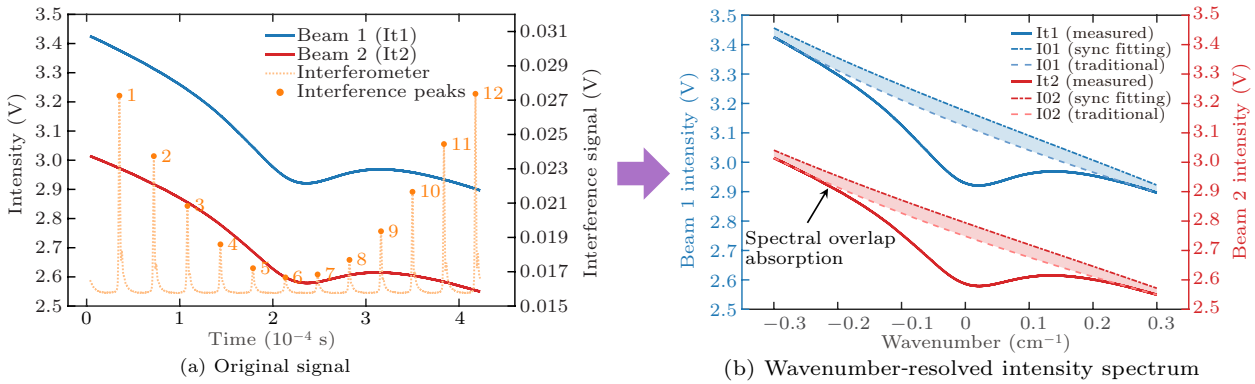


Fig. 9. Time–frequency signal conversion and fitted baseline: (a) raw time-domain signal, (b) fitted baseline and absorbance spectrum.

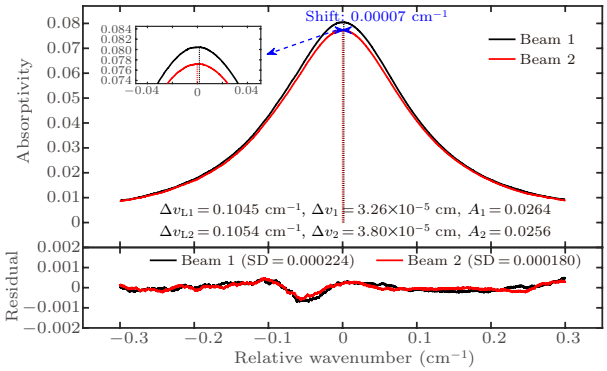


Fig. 10. Dual spectral line fitting under zero-flow conditions.

The absorption spectra for both laser beams were precisely fitted using the procedure in Fig. 3 to extract the relative Doppler shift. Figure 10 shows the fitting results for the two spectral lines under zero-flow conditions. The standard deviation of the overall residual from repeated spectral fitting experiments ranged between 1.8×10^{-4} cm^{-1} and 2.3×10^{-4} cm^{-1}. Ideally, the spectral lines should perfectly overlap under zero flow, yielding zero frequency shift. And both spectral lines should exhibit zero Doppler shift ($\Delta\nu = 0$) under zero-flow conditions. However, consistent non-zero velocity outputs of approximately 1.24 m/s were observed across multiple measurements. This zero-point deviation primarily originates from temporal phase offset between the two signal acquisition channels. Although both laser beams are generated from the same DFB laser source with identical wavelength modulation, the data acquisition card exhibits inherent channel-to-channel skew, a small but fixed temporal difference in sampling moments between the two channels. During rapid wavelength scanning, this temporal offset causes the two

channels to sample signals at slightly different instantaneous laser wavelengths, which manifests as an apparent wavenumber difference between the two spectral lines after time-to-wavelength conversion.[31]

Long-term continuous measurements (Fig. 12) confirm that this deviation is highly reproducible and stable throughout extended measurement periods, indicating its systematic nature originating from a fixed temporal offset rather than random fluctuations. The zero-point deviation consists of a fixed systematic offset of approximately 1.24 m/s superimposed with a smaller fluctuating component (standard deviation 0.6 m/s), with the latter partially attributed to variations in absorption conditions affecting synchronous fitting results. This systematic deviation is corrected through zero-flow calibration, where the measured offset is subtracted from all velocity calculations to eliminate the influence of temporal phase offset.

Under ideal conditions, both absorption spectra should exhibit identical scalar characteristics (*e.g.*, Lorentzian width $\Delta\nu_C$, absorbance A) but opposite frequency shifts. However, as evident from the fitting parameters in Fig. 11, deviations in these scalar parameters occurred in the experiment. These discrepancies primarily stem from turbulence effects and the presence of stagnant zones during measurement, causing the detector to receive superposed absorption lines rather than an ideal single line. This superposition induces spectral distortion, reducing single-line fitting accuracy and ultimately degrading velocity measurement precision.

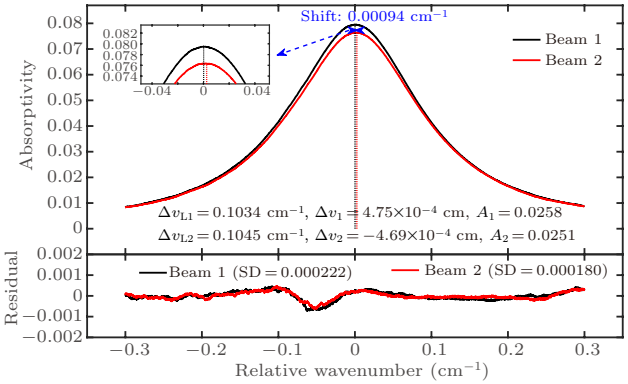


Fig. 11. Dual spectral line frequency shift at 23.63 m/s flow velocity.

For comprehensive validation, continuous measurements were conducted for 5 minutes under each flow condition. Each measurement, which included both signal acquisition and subsequent processing, took 0.25 s to complete. This approach yields approximately 1200 data points per condition, providing robust statistical characterization of measurement performance and long-term stability. For three distinct fan power settings, the Pitot tube measured centerline velocities V_{max} were 13.66 m/s, 28.23 m/s, and 40.96 m/s. Based on the flow field non-uniformity analysis (Subsection 4.1), the path-averaged velocities along the TDLAS beam were calculated as 8.46 m/s, 17.50 m/s, and 25.42 m/s, respectively. Figure 12 presents the continuous measurement results for four flow conditions (group 1: zero flow; groups 2–4: increasing fan speed settings). Scatter points represent individual velocity measurements, solid black lines show moving averages calculated over 100-point windows, and dashed lines indicate 95% confidence intervals. In group 1, the TDLAS measurement shows 1.24 m/s with standard deviation of 0.60 m/s. This deviation is attributed to temporal phase offset between the two signal acquisition channels. The high reproducibility of this offset (stable around 1.24 m/s throughout the 5-minute measurement period) confirms its systematic nature.

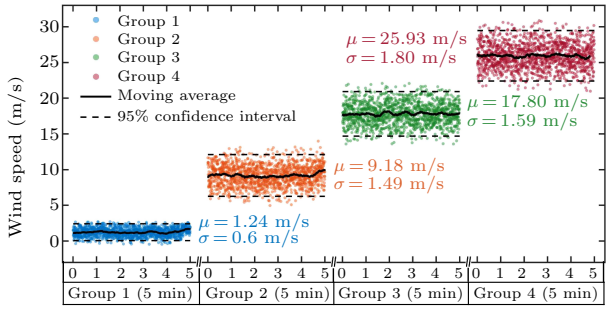
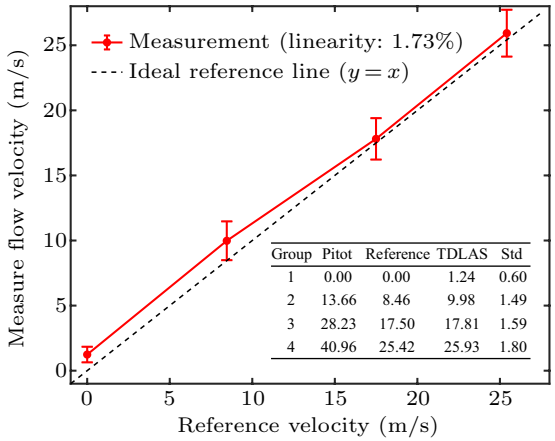


Fig. 12. Continuous online measurement results for four flow velocity groups.

After zero-flow calibration, TDLAS measurements for groups 2–4 are 9.18 m/s, 17.80 m/s, and 25.93 m/s, respectively. The moving average lines maintain remarkable stability throughout the 5-minute periods with minimal drift ($<$ 0.5 m/s), confirming the long-term stability and robustness of the synchronous fitting algorithm during continuous operation. The standard deviations of measurements for each group are 0.6 m/s, 1.49 m/s, 1.59 m/s, and 1.80 m/s, respectively, quantifying the typical scatter of individual measurements around their mean values. The increase in standard deviation with flow velocity indicates that enhanced turbulence at higher flow rates leads to greater dispersion in velocity measurements, resulting in a broader distribution of measured values.

Figure 13 compares the TDLAS-measured flow velocities (after zero-flow calibration) with path-averaged reference velocities. The overall relative error of the TDLAS velocity measurements remains below 10% when compared to the radially averaged velocity derived from the power-law distribution model. Furthermore, the system exhibits excellent linearity, with a linearity of 1.73%. These results demonstrate that the TDLAS measurement system possesses excellent performance and consistency in low-speed flow fields, with the expanded dataset providing comprehensive validation of long-term stability and reliability.



Group	Pitot	Reference	TDLAS	Std
1	0.00	0.00	1.24	0.60
2	13.66	8.46	9.98	1.49
3	28.23	17.50	17.81	1.59
4	40.96	25.42	25.93	1.80

Fig. 13. Comparison of velocity measurements: TDLAS *versus* Pitot tube.

5. Conclusion

This study presents comprehensive theoretical and experimental investigations of gas velocity measurements in low-speed flow fields (0–30 m/s) using tunable diode laser absorption spectroscopy (TDLAS). To overcome the challenge of minute Doppler shifts ($< 1.5 \times 10^{-3}$ cm^{-1}) in low-speed flows, we developed a high-precision synchronous iterative fitting algorithm with L2-norm constraint. This approach enables simultaneous optimization of baseline and absorbance parameters, effectively mitigating baseline drift while resolving extraction difficulties caused by overlapping water vapor (H_2O) absorption lines, thereby yielding absorption spectra with enhanced accuracy. A dual-light-path TDLAS platform was constructed, targeting the H_2O absorption line at 7181.1557 cm^{-1} with a 100° beam crossing angle. Integrated with a LabVIEW-controlled data acquisition system, the setup enables continuous real-time measurements at a cycle of 0.25 s. A power-law velocity distribution model was applied to convert Pitot tube point measurements into path-averaged velocities, accounting for flow non-uniformity in cylindrical pipes. Validation via 5-minute continuous tests under varied flow conditions confirmed system robustness across 0–30 m/s. After zero-flow calibration to correct channel phase offsets, the system achieved relative errors below 10% and a linearity of 1.73%. Long-term stability was demonstrated by minimal drift (< 0.5 m/s) in moving averages over extended durations. In summary, this work systematically establishes technical foundations for TDLAS-based low-speed flow diagnostics, providing critical insights for engineering applications and real-time multi-parameter monitoring. Future research should focus on enhancing signal-processing robustness and optimizing beam-path configurations to extend the measurement range and accuracy.

Acknowledgements

Project supported by the National Natural Science Foundation of China (Grant No. 52276005) and the Beijing Natural Science Foundation (Grant No. 3232036).

References

[1] Jung S, Shim H, Kim G, *et al.* 2023 *J. Mech. Sci. Technol.* **37** 4099
[2] Fu M, Zhang H Z, Yin J F, *et al.* 2020 *J. Propul. Technol.* **41** 2130
[3] Wecel D, Chmielniak T and Kotowicz J 2008 *Flow Meas. Instrum.* **19** 301
[4] Sheng S Z, Zhuang Y J and Liu Z Y 2009 *J. Exp. Fluid Mech.* **23** 89
[5] Zhang D, Zhou W, Tropea C, *et al.* 2025 *Exp. Fluids* **66** 107
[6] Li J W, Luo K, Shang J H, *et al.* 2024 *Chin. J. Theor. Appl. Mech.* **56** 890
[7] Reid J and Labrie D 1981 *Appl. Phys. B* **26** 203
[8] Albrecht H E, Borys M, Damaschke N and Tropea C 2003 *Laser Doppler and Phase Doppler Measurement Techniques* (Berlin: Springer-Verlag)
[9] Hanson R K, Spearrin R M and Goldenstein C S 2016 *Spectroscopy and Optical Diagnostics for Gases* (Cham: Springer)
[10] Philippe L C and Hanson R K 1993 *Appl. Opt.* **32** 6090
[11] Wehe S D, Baer D S, Hanson R K and Chadwick K M 1998 *AIAA Paper* **98** 2699
[12] Yang B, He G G, Liu P J, *et al.* 2011 *Laser Technol.* **35** 503
[13] Tu R, Gu J, Zeng Y, Zhou X, Yang K, Jing J, Miao Z and Yang J 2022 *Sensors* **22** 6707
[14] Lu F, Cao Z, Chang L, Zhao K, Xue X, Lin Y and Xu L 2024 *IEEE Trans. Instrum. Meas.* **73** 6009611
[15] Zhou W, Cao Z, Dou S, Duan X, Yang Q and Xu L 2025 *Measurement* **241** 115716
[16] Lyle K H, Jeffries J B and Hanson R K 2007 *AIAA J.* **45** 2213
[17] Reid J and Labrie D 1981 *Appl. Phys. B* **26** 203
[18] Liu C and Xu L 2019 *Appl. Spectrosc. Rev.* **54** 1
[19] Li W 2018 *Research and Application of a Velocity Measurement System Based on Laser Doppler Effect*, MS Dissertation (Nanjing: Nanjing University of Science and Technology)
[20] Gordon I E, *et al.* 2017 *J. Quant. Spectrosc. Radiat. Transfer* **203** 3
[21] Ma L, Ning H, Wu J and Ren W 2018 *Combust. Sci. Technol.* **190** 392
[22] Xu Z Y, Liu W Q, Kan R F, *et al.* 2010 *Spectrosc. Spect. Anal.* **30** 2201
[23] Goldenstein C S, Spearrin R M, Jeffries J B and Hanson R K 2014 *Appl. Phys. B* **116** 705
[24] Schlichting H and Gersten K 2000 *Boundary-Layer Theory*, 8th edn. (Berlin: Springer)
[25] Durbin P A and Pettersson Reif B A 2011 *Statistical Theory and Modeling for Turbulent Flows*, 2nd edn. (Chichester: Wiley)
[26] White F M 2006 *Viscous Fluid Flow*, 3rd edn. (New York: McGraw-Hill)
[27] Pope S B 2000 *Turbulent Flows* (Cambridge: Cambridge University Press)
[28] Tennekes H and Lumley J L 1972 *A First Course in Turbulence* (Cambridge: MIT Press)
[29] Nikuradse J 1932 *Forsch. Ing.-Wes.* **3** 1
[30] Barenblatt G I 1993 *J. Fluid Mech.* **248** 513
[31] Hanson R K, *et al.* 2011 *Appl. Opt.* **50** A47